Biphasic Peptide Amphiphile Nanomatrix Embedded with Hydroxyapatite Nanoparticles for Stimulated Osteoinductive Response

Joel M. Anderson,[†] Jessica L. Patterson,[†] Jeremy B. Vines,[†] Amjad Javed,[‡] Shawn R. Gilbert,[§] and Ho-Wook Jun*,[†]

[†]Department of Biomedical Engineering, [‡]Institute of Oral Health Research, and [§]Department of Surgery, University of Alabama at Birmingham, Birmingham, Alabama 35294-2182, United States

ABSTRACT Formation of the native bone extracellular matrix (ECM) provides an attractive template for bone tissue engineering. The structural support and biological complexity of bone ECM are provided within a composite microenvironment that consists of an organic fibrous network reinforced by inorganic hydroxyapatite (HA) nanoparticles. Recreating this biphasic assembly, a bone ECM analogous scaffold comprising self-assembling peptide amphiphile (PA) nanofibers and interspersed HA nanoparticles was investigated. PAs were endowed with biomolecular ligand signaling using a synthetically inscribed peptide sequence (*i.e.,* RGDS) and integrated with HA nanoparticles to form a biphasic nanomatrix hydrogel. It was hypothesized the biphasic hydrogel would induce osteogenic differentiation of human mesenchymal stem cells (hMSCs) and improve bone healing as mediated by RGDS ligand signaling within PA nanofibers and embedded HA mineralization source. Viscoelastic stability of the biphasic PA hydrogels was evaluated with different weight concentrations of HA for improved gelation. After demonstrating initial viability, long-term cellularity and osteoinduction of encapsulated hMSCs in different PA hydrogels were studied *in vitro*. Temporal progression of osteogenic maturation was assessed by gene expression of key markers. A preliminary animal study demonstrated bone healing capacity of the biphasic PA nanomatrix under physiological conditions using a critical size femoral defect rat model. The combination of RGDS ligand signaling and HA nanoparticles within the biphasic PA nanomatrix hydrogel demonstrated the most effective osteoinduction and comparative bone healing response. Therefore, the biphasic PA nanomatrix establishes a well-organized scaffold with increased similarity to natural bone ECM with the prospect for improved bone tissue regeneration.

KEYWORDS: peptide amphiphile · hydroxyapatite · osteogenic differentiation · human mesenchymal stem cells · hydrogel · biomimetic

The development of biomaterials for bone regeneration has progressively focused on directing cellular response for new tissue formation using a biomimetic approach. Exploiting natural tissue self-assembly as an architectural template, it is critical to design materials that provide specific biomolecular signaling within a hierarchically organized framework similar to physiological conditions. Adapting this strategy to tissue engineered bone solutions remains a challenge, propagated by an inability to fully reconstitute synthetically derived local microenvironments that resemble the natural bone extracellular matrix (ECM). Native ECM serves as a complex structural network surrounding cells for support and providing regulation of intracellular communication and dynamic cellular response through cell-ECM ligand interactions.[1,2] The bone ECM microenvironment consists of organic matrix rich collagen fibers reinforced by inorganic hydroxyapatite (HA) nanocrystals, serving as a composite interface for local osteogenic cells.[3,4] Most biomaterials for bone tissue engineering differ from bone in either compositional structure or bioactive signaling because of a tendency to be single-phase materials, often ignoring one of these two essential features.[4] Thus, there is a great need to engineer biomaterials analogous to the structural and biological characteristics of native bone, specifically the fundamental bone ECM, to create a biomimetic microenvironment with an instructive capacity for regeneration at the cellular level that can be effectively translated to *in vivo* bone repair.

Efforts to synthetically recreate the bone ECM microenvironment within a tissue engineered hydrogel are prevalent, typically utilizing a fibrous scaffold assembly. For example, synthetic hydrogels for bone tissue applications have included polymethacrylate, polyethylene glycol, and oligo (polyethylene glycol) fumarate.[5−8] While these synthetic materials provide precise scaffold control of physical properties, it is often difficult to readily encapsulate cells under physiological conditions *via* self-assembly

* Address correspondence to hwjun@uab.edu.

Received for review June 27, 2011 and accepted November 11, 2011.

Published online November 11, 2011
10.1021/nn203247m

mechanisms similar to native ECM formation. At the same time, challenges persist in incorporating bioactive ligands to mimic ECM signaling functionality within a biodegradable network. As a potential solution, self-assembling peptide-based scaffolds offer the promise of realized three-dimensionality within a nanofibrous network, diffusion capability, cell responsive degradation for native tissue in-growth, and instructive biological signaling synthetically derived from tissue-specific ECM molecules.[9]

To this point, the peptide amphiphile (PA) has been developed as a bioactive material capable of self-assembly into high aspect ratio nanofibers that mimic the fibrous ECM nanostructure.[10,11] The PA molecule is composed of a charged amino acid sequence covalently attached to a hydrophobic aliphatic chain, which enables nanofiber self-assembly due to hydrophobic collapse of the alkyl tails.[10,12,13] Self-assembly of PA nanofibers is initiated by the screening of charged groups, typically facilitated by pH change or the addition of multivalent ions under physiological conditions.[11,14] Upon induction, the PAs produce self-assembled cylindrical nanostructures with exposed bioactive peptide signals on the outer periphery. The resulting PA nanofibers are able to form robust non-covalent cross-links between fibers, creating an interwoven nanomatrix that gives rise to a macroscopic self-supporting hydrogel.[15,16] By modifying the peptide sequence, PAs can be customized for many different tissue engineering purposes. Our laboratory has adapted the PA molecule for applications in osteogenic differentiation, endothelium and cardiovasculature, pancreatic islet engraftment, hybrid scaffolding, tunable gelation, and drug delivery.[17−25] However, the development of a biphasic PA nanomatrix that recapitulates the organic/inorganic composite of native bone ECM by internally incorporating a HA mineralization source within the nanofiber network has yet to be fully investigated, especially in regards to bone tissue regeneration *in vivo*.

HA is the major inorganic mineral constituent of bone ECM, occurring naturally as a nanocrystalline structure for mineralization in the osseous microenvironment.[4,26] Recently, HA has begun to take hold as a composite scaffolding material, commonly combined with other bulk biomaterials to provide the lacking inorganic phase.[4,27−30] HA composites have demonstrated excellent biocompatibility and can even increase stability and other mechanical properties in a controllable manner, improving scaffold integrity and handling for biomaterial implantation.[4,31] Additionally, there is emerging evidence that the inclusion of HA can increase osteoinduction; though, this remains a contentious issue that is not yet fully understood.[32−34] Thus, it is believed the inclusion of HA in a PA nanomatrix has the potential to further improve upon composite scaffold design by combining an inorganic mineral source with a self-assembling ECM mimetic fibrous structure endowed with biological signaling and cell responsive degradation. The goal of this multifaceted scaffold is to create an osteoinductive microenvironment that effectively approximates the natural bone ECM at the nanostructured level of tissue formation. This biomimetic assembly would thereby establish a biphasic nanomatrix of organic PA nanofibers interspersed with inorganic HA nanoparticles to be investigated for induced osteogenic differentiation and long-term bone tissue regeneration.

In our previous work, we demonstrated that tailored PAs have the capacity for guided osteogenic differentiation based on synthetic cell-ligand interactions, as specific ECM ligand signals were synthetically inscribed into the outer peptide domain.[18] Furthermore, we have created viscoelastically tunable PA nanomatrix hydrogels by coassembling two functionally specific PAs with differing gelation properties at precise ratios, developing a controllable system for gel stability with maintained bioactive signaling.[17] From these studies, the RGDS (Arg-Gly-Asp-Ser) ligand, prevalent in ECM molecules such as fibronectin and laminin, was found to be the most osteoinductive peptide sequence. This is supported by previous studies showing the osteoinductive signaling potential of the RGDS ligand.[35−37] Thus, for this work, the same PA molecule structure has been maintained, consisting of a hydrophobic alkyl tail linked to hydrophilic peptide segment of inscribed ECM ligand and internal matrix metalloproteinase-2 (MMP-2) enzyme-degradable sequence. Two different PAs were synthesized, with the RGDS ligand being chosen for further investigation as an osteoinductive signal within the biphasic PA nanomatrix, along with a biologically inert (serine residue) placeholder as the negative control. This provided an attractive self-assembling hydrogel template for combining with HA to achieve a well-organized construction with an increased similarity to natural bone ECM. It was hypothesized that the biphasic PA nanomatrix would induce stimulated osteogenic differentiation of human mesenchymal stem cells (hMSCs) directed by the inscribed bioactive ligand sequence within the PAs and embedded HA nanoparticles for improved bone tissue regeneration. Experimentally, the biphasic PA nanomatrix hydrogels were developed and tested for viscoelastic stability with different HA concentrations, induction of nanofiber self-assembly, initial cellular viability, long-term cellularity, osteogenic potential by gene expression of phenotypic markers, and *in vivo* healing response of a critical size femoral defect *via* a preliminary animal study. This work thereby offers one of the first approaches to innovatively combine and investigate multifaceted scaffolds analogous to the self-assembled formation of native bone tissue for

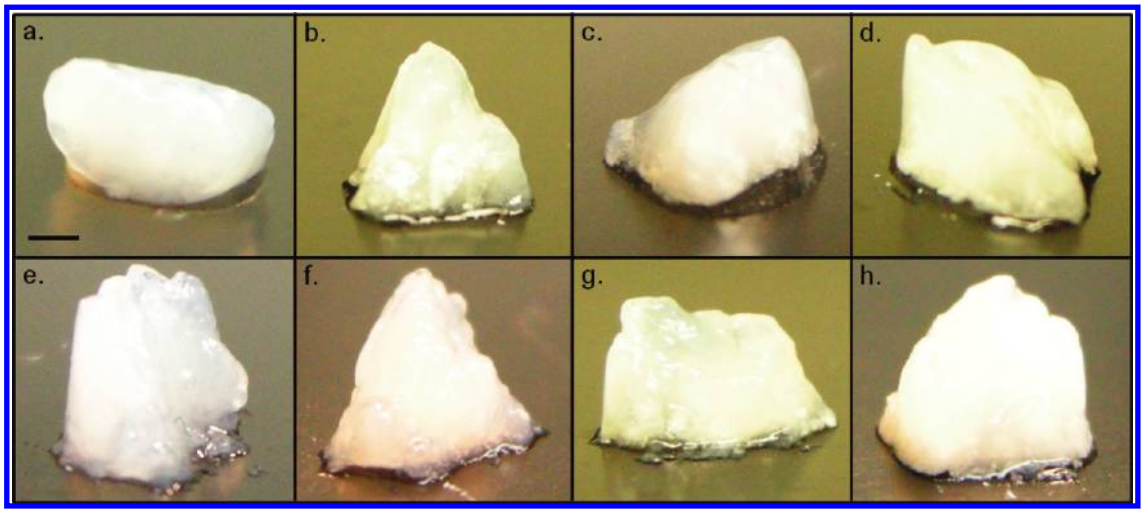

Figure 1. Macroscopic PA hydrogel images of (a–d) PA-RGDS/PA-S (1:1) and (e–h) PA-S. Biphasic PAs created by self-assembling hydrogels with different HA concentrations: (a,e) 0%, (b,f) 33.3%, (c,g) 50%, and (d,h) 66.7%. HA concentrations (%) calculated as percentage of added HA mass to total hydrogel mass (HA + PA). Scale bar represents 1 mm.

TABLE 1. Ratio of Storage Modulus to Loss Modulus for Biphasic Peptide Amphiphile Hydrogels

	G'/G''[a]	
HA % concentration	PA-RGDS/PA-S (1:1)	PA-S
0	4.085 ± 0.81	5.958 ± 0.16
33.3	3.939 ± 1.26	4.541 ± 0.72
50	8.494 ± 0.71*	9.701 ± 0.34*
66.7	4.594 ± 0.89	6.688 ± 0.38

[a] Ratio of storage modulus (G') to loss modulus (G'') at 10 Hz. * Significantly greater than all other HA concentrations ($p < 0.05$).

tissue regenerative applications with great promise for clinical translation.

RESULTS

Gelation and Viscoelastic Properties. The two PAs were successfully synthesized and verified to have correct molecular weights prior to calcium divalent ion induced self-assembly into nanomatrix hydrogels. This included both the bioactive PA inscribed with RGDS ligand signaling (*i.e.,* PA-RGDS) and corresponding negative control PA sequence (*i.e.*, PA-S) in which the outer domain was replaced with an inert serine residue placeholder. On the basis of previous work, PA-RGDS was coassembled with the stronger gelating PA-S sequence at a molar ratio (Mr_{PA-S} = PA-RGDS/PA-S) of 1:1 to provide needed stability, while still maintaining bioactive ligand signaling, and designated as PA-RGDS/PA-S (1:1).[17] To first develop the biphasic PA composites, it was important to determine the appropriate amount of HA content to include within the self-assembling nanomatrix based on gelation and viscoelastic stability for increased handling and durability as an implantable biomaterial. PA-RGDS/PA-S (1:1) and PA-S were self-assembled into hydrogels embedded with many different HA weight concentrations: 0%, 33.3%, 50%, and 66.7%. As depicted in Figure 1, the macroscopic gel quality was observed for both PA-RGDS/PA-S (1:1) and PA-S with different concentrations of HA nanoparticles. All biphasic PA hydrogels were found to be self-supporting and successfully retain the embedded HA, regardless of HA concentration or PA sequence.

The viscoelastic properties of the different biphasic composites were then evaluated using dynamic oscillatory rheometry in which the storage (G') and loss (G'') moduli were monitored as a function of frequency sweep measurements at low strain amplitude. Storage and loss moduli are respective measures of the ability to store and dissipate deformation energy during loading, and an increasing ratio of storage modulus to loss modulus (G'/G'') is a key indicator of stronger elasticity in hydrogels, as opposed to viscous liquids.[38,39] As demonstrated in Table 1, increasing the HA concentration within the biphasic PA hydrogels greatly improved the observed ratios of G'/G'' before oversaturation at 66.7% HA caused a drop-off. The G'/G'' ratios for both PA-RGDS/PA-S (1:1) and PA-S hydrogels were greatest at the 50% HA weight concentration, exhibiting values approximately twice their control gel (0%) counterparts containing no HA and indicating predominant elastic gel character at this biphasic condition. Therefore, the viscoelastic properties of PA hydrogels can be directly controlled by embedding different amounts of HA nanoparticles, as increasing concentration led to greater viscoelasticity up to a certain point. The most viscoelastically stable gels, comparatively, were found to be the 50% HA weight concentration for both PA sequences before the interactions between polymer and mineral did not transfer the viscoelastic load as effectively at the highest

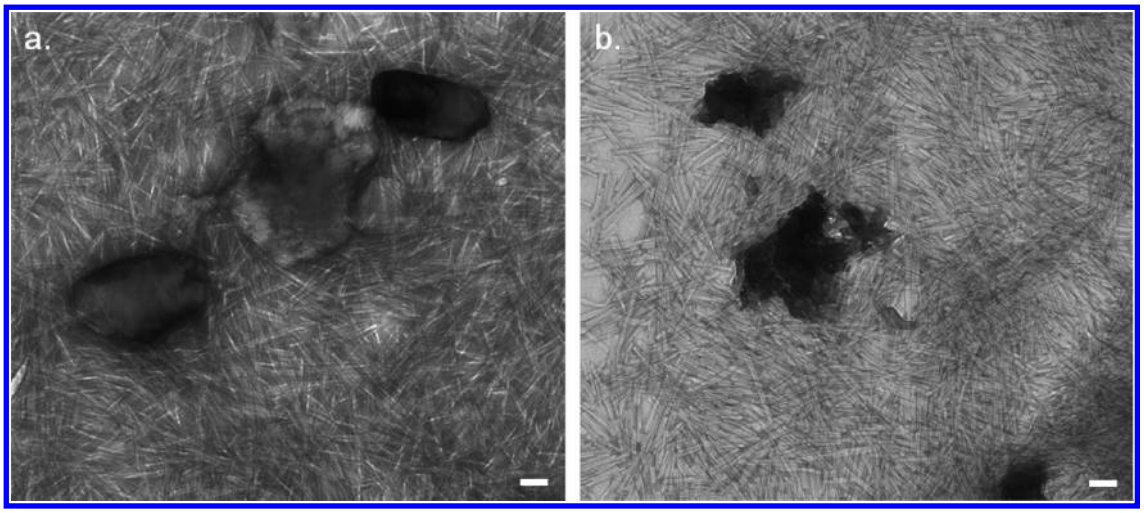

Figure 2. TEM images of biphasic PA hydrogels self-assembled with 50% HA concentration in (a) PA-RGDS/PA-S (1:1) and (b) PA-S. Scale bar represents 100 nm.

concentration, resulting in a decrease in the G'/G'' ratios. Consequently, the HA weight concentrations for the biphasic PA nanomatrix hydrogels were fixed at 50% for all further experiments.

TEM Imaging of Nanostructure. Accordingly, the biphasic PA nanomatrix hydrogels were self-assembled at only the 50% HA weight concentration for transmission electron microscope (TEM) imaging, excluding all other HA concentrations. Both PA-RGDS/PA-S (1:1) and PA-S underwent induced nanofiber self-assembly after the addition of divalent calcium ions, embedding HA nanoparticles within the nanofibrous networks. On the basis of TEM imaging (Figure 2), the observed nanostructures for both biphasic hydrogels showed that PA nanofiber self-assembly was unaffected by the inclusion of HA nanoparticles at the 50% weight concentration. Consistent nanofibrous PA formations were evident throughout, composed of cylindrical micelle nanostructures in the range of 6−10 nm diameters and lengths approaching several micrometers. The observed nanofiber morphology and formation are consistent with past studies performed without HA.[10,16,17] Thus, dispersed HA nanoparticles can be effectively integrated into self-assembling PAs to create biphasic nanomatrices.

Cellular Viability. hMSCs were encapsulated in the different combinations of PA nanomatrix hydrogels for 3 days. The initial viability was qualitatively observed by Live/Dead fluorescent staining of encapsulated cells in PA-RGDS/PA (1:1) and PA-S, with HA embedded at both 0% and 50% concentrations (Figure 3). Representative images showed high levels of hMSC viability for all PA nanomatrix conditions, indicated by the abundance of positive green fluorescence. In particular, the biphasic PA hydrogels demonstrated excellent cellular biocompatibility, regardless of peptide sequence or HA inclusion. Thus, the embedded HA nanoparticles did not negatively affect hMSC viability in the self-assembled hydrogels. All PA hydrogels cultivated high levels of cell confluency with well-defined morphology for growth and migration. Furthermore, the encapsulated cells within the PA hydrogels demonstrated pervasion of viable hMSCs throughout the three-dimensional gel geometries, as imaged from the bottom-up by confocal microscopy.

Cellularity. For progenitor cells to differentiate along an osteogenic lineage, maintained cellularity over long-term *in vitro* incubation is needed. In addition to ensuring sufficient cellular retention in the biphasic PA hydrogels, a shift from proliferative to differentiated phenotypic state is likely to first be detected by an observed plateau in cell proliferation.[40] Taking this into consideration, the long-term cellularity of hMSCs incubated in the PA nanomatrix hydrogels with and without HA (50% weight concentration) was evaluated over 28 days *in vitro* (Figure 4). The initial cellular retention at day 0 was significantly greater for PA-RGDS/PA-S (1:1), 0% HA compared to the biphasic hydrogels at the same time point. However, the greatest proliferation in cellularity over the initial amount was observed for the biphasic PA-RGDS/PA-S (1:1), 50% HA hydrogel at each subsequent time point, followed by PA-RGDS/PA-S (1:1), 0% HA and PA-S, 50% HA, which also both promoted significantly increased proliferation at days 7 and 14. Consequently, the biphasic PA-RGDS/PA-S (1:1), 50% HA hydrogel exhibited significantly greater cellularity over both PA-S hydrogels, regardless of HA inclusion, for days 7 and 14. The same held true for PA-RGDS/PA-S (1:1), 0% HA at day 14, as greater cellularity was observed compared to the negative control hydrogels (containing PA-S). Both RGDS ligand-containing PA nanomatrix hydrogels were more effective mediators of cellularity, similar to findings in previous studies.[18,41] Moreover, embedded HA in combination with PA-RGDS/PA-S (1:1) was found to further increase cellularity compared to its single-phase

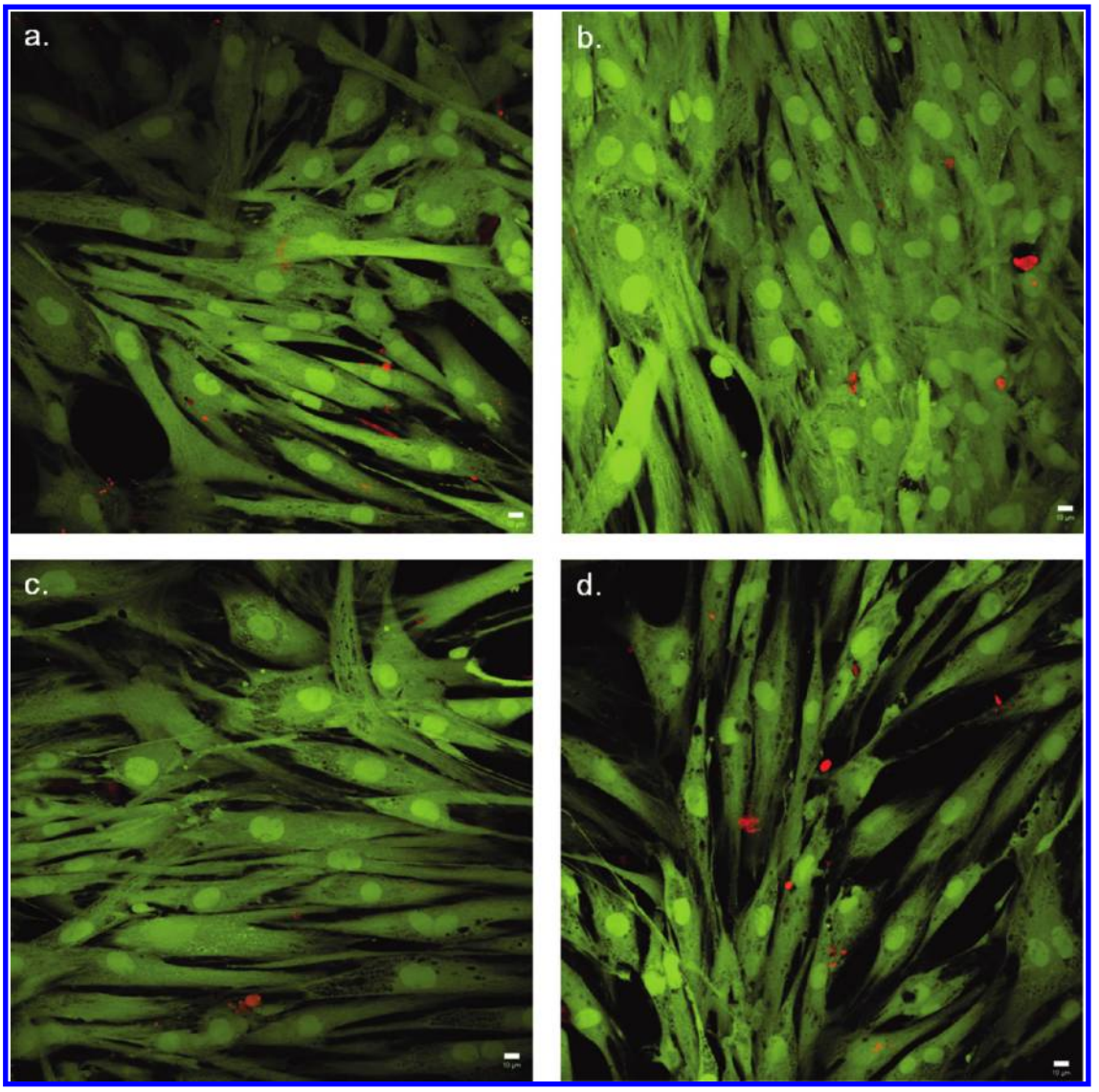

Figure 3. Representative Live/Dead fluorescent images of hMSCs encapsulated in (a,b) PA-RGDS/PA-S (1:1) and (c,d) PA-S after 3 days. Both PA hydrogels were imaged with embedded HA concentrations of (a,c) 0% and (b,d) 50%. Viewed under confocal microscopy, viable cells fluoresce green, and dead cells are red. Scale bar represents 10 μm.

counterpart, as evidenced by the greatest peaks in cell number over the majority of the incubation. Overall, all PA nanomatrix hydrogels demonstrated long-term cellular retention of 30−40% of the initially encapsulated cells, maintaining a density of approximately 15000 cells/hydrogel over 28 days for all gel conditions. Thus, sufficient cellularity of hMSCs was maintained long-term in all biphasic PA hydrogels, enabling extended observations of osteogenic differentiation.

Quantitative Real-Time PCR Gene Expression. Osteoinduction was next quantified using real-time PCR gene expression, assessing the promoted levels of osteogenic maturation expressed by hMSCs as influenced by the encapsulating PA nanomatrices over 28 days *in vitro*. Gene expression was analyzed utilizing several different target markers, including Runx2, alkaline phosphatase (ALP), collagen type I, and osteocalcin (OCN). Phenotypic expression over the entire temporal progression of osteogenic differentiation starts with the transcription factor Runx2, which is responsible for inducing downstream expression of intermediate and late-stage markers.[42,43] ALP and collagen type I serve as two of the main intermediate markers in the differentiation process, pivotal to preparations of the ECM for subsequent terminal mineralization;[44] at which time, OCN is maximally expressed as a late-stage marker.[45] Furthermore, the quantified gene expression values for all target markers were normalized to the internal standard of β-actin to allow for relative comparisons. Thus, evaluation of normalized phenotypic markers that span the entire osteoinductive gene expression profile was achieved.

As shown in Figure 5, Runx2 gene expression was first quantified for all PA nanomatrix hydrogels. After similar relative values at day 0, significantly greater Runx2 expression was observed for PA-RGDS/PA-S

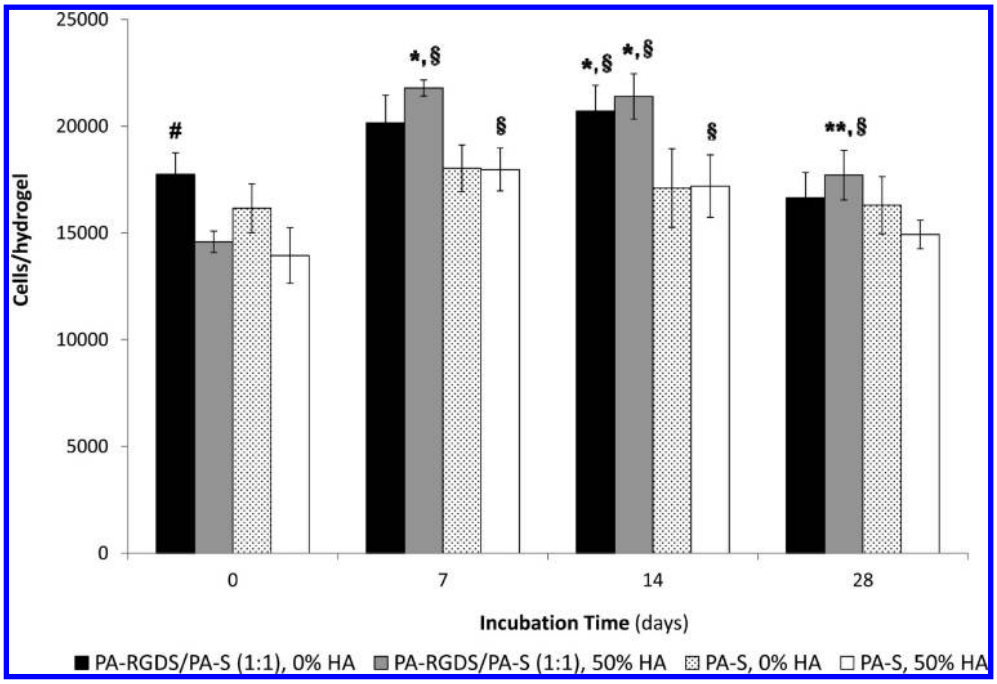

Figure 4. Cellularity of hMSCs over 28 days. (#) PA-RGDS/PA-S (1:1), 0% HA promoted significantly greater cellularity than PA-RGDS, 50% HA and PA-S, 50% HA at day 0. (∗) PA-RGDS/PA-S (1:1), 0% HA and PA-RGDS/PA-S (1:1), 50% HA exhibited greater cellularity than both PA-S, 0% HA and PA-S, 50% HA per time point. (∗∗) A-RGDS/PA-S (1:1), 50% expressed higher cellularity than PA-S, 50% HA at day 28. (§) Samples significantly increased in cellularity compared to day 0 ($p < 0.05$).

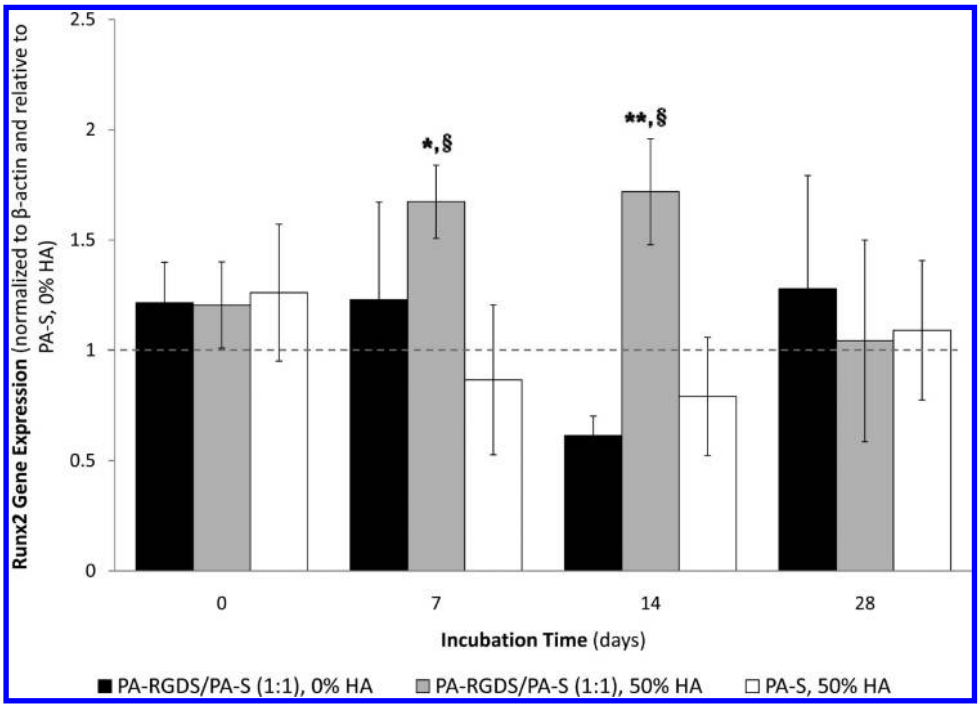

Figure 5. Gene expression profile for Runx2 over 28 days. Values expressed as mean ± standard deviation relative to PA-S, 0% HA (dashed line) for each time point. PA-RGDS/PA-S (1:1), 50% HA promoted significantly greater expression than (∗) PA-S, 50% HA on day 7, (∗∗) PA-RGDS/PA-S (1:1), 0% HA and PA-S, 50% HA on day 14, and (§) normalization control of PA-S, 0% HA ($p < 0.05$).

(1:1), 50% HA compared to both negative control PA-S hydrogels at day 7. Continued up-regulation of Runx2 was promoted by the same biphasic RGDS-mediated PA on day 14, evidenced by higher relative expression than all other PA conditions. This early up-regulation of Runx2 gave way to the heightened gene expression of ALP halfway through incubation, coinciding with the leveling out of Runx2 beyond the first two weeks.

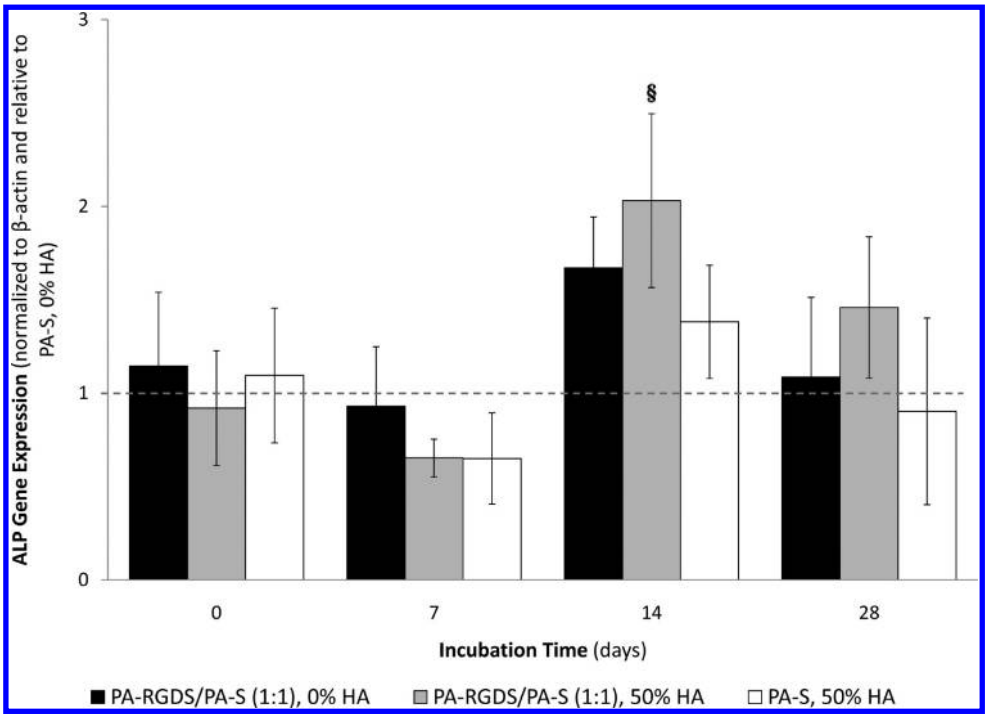

Figure 6. Gene expression profile for ALP over 28 days. Values expressed as mean ± standard deviation relative to PA-S, 0% HA (dashed line) for each time point. (§) PA-RGDS/PA-S (1:1), 50% HA promoted significantly greater expression than the normalization control of PA-S, 0% HA ($p < 0.05$).

Specifically, PA-RGDS/PA-S (1:1), 50% HA exhibited significantly greater ALP gene expression over PA-S, 0% HA at the day 14 time point, while ALP expression remained unchanged at all other incubation periods across tested samples (Figure 6). This was followed by gene expression analysis of collagen type I, as depicted in Figure 7. Again, PA-RGDS/PA-S, 50% HA significantly up-regulated target gene expression, promoting an increased collagen type I profile for days 14 and 28. In particular, collagen type I gene expression elicited by the PA-RGDS/PA-S, 50% HA nanomatrix dramatically increased over the last two weeks of incubation based on much higher relative values compared to all other PA conditions. Concluding the temporal progression of osteoinduction, the late-stage phenotypic marker of OCN was quantified (Figure 8). Gene expression of OCN was significantly up-regulated by both PA nanomatrix hydrogels containing the RGDS ligand. At day 14, the biphasic PA-RGDS/PA-S, 50% HA hydrogel promoted significantly greater OCN expression relative to all other PA hydrogels. Increased OCN expression was maintained at day 28 for the biphasic RGDS-containing PA; however, the single-phase PA-RGDS/PA-S, 0% HA hydrogel had overtaken all other conditions in observed expression, indicating a slight delay in OCN phenotypic display as mediated by the RGDS ligand without HA. Overall, the biphasic PA-RGDS/PA-S (1:1), 50% HA hydrogel best induced osteogenic differentiation of hMSCs based on relative gene expression of phenotypic markers covering all stages of the maturation process. The combination of bioactive RGDS ligand and HA nanoparticles within the self-assembled PA nanomatrix hydrogel proved to be a more potent mediator of osteoinduction compared to all other PA conditions, after all initially started out together at the same relative expression levels. However, the PA-RGDS/PA-S (1:1) hydrogel by itself (0% HA) also demonstrated increased osteoinductivity that surpassed the negative control PA-S hydrogels, regardless of HA inclusion, indicating the inductive signaling potential of the RGDS ligand.

Lastly, MMP-2 gene expression was quantified for all PA hydrogels. MMP-2 serves as a highly conserved enzyme secreted from inside the cell to the cell surface, where it degrades most components of the basement membrane and ECM.[46] The inclusion of the MMP-2 sensitive sequence within the internal peptide structure of all PAs adds a vital biodegradation component to enable native tissue in-growth. As shown in Figure 9, MMP-2 gene expression exhibited by encapsulated hMSCs was unaffected for all PAs evaluated, including the biphasic conditions containing HA. Over 28 days cultivation *in vitro*, MMP-2 expression levels remained at the same relative values for all the different PA hydrogels. This verifies consistent MMP-2 expression by the encapsulated hMSCs throughout the study, enabling unbiased cell-mediated proteolytic degradation and potential for cell migration within the nanomatrix hydrogels.

Radiographic Analysis. New bone formation in a pilot animal study was first evaluated qualitatively by radiographic X-ray images to assess clinical effectiveness of

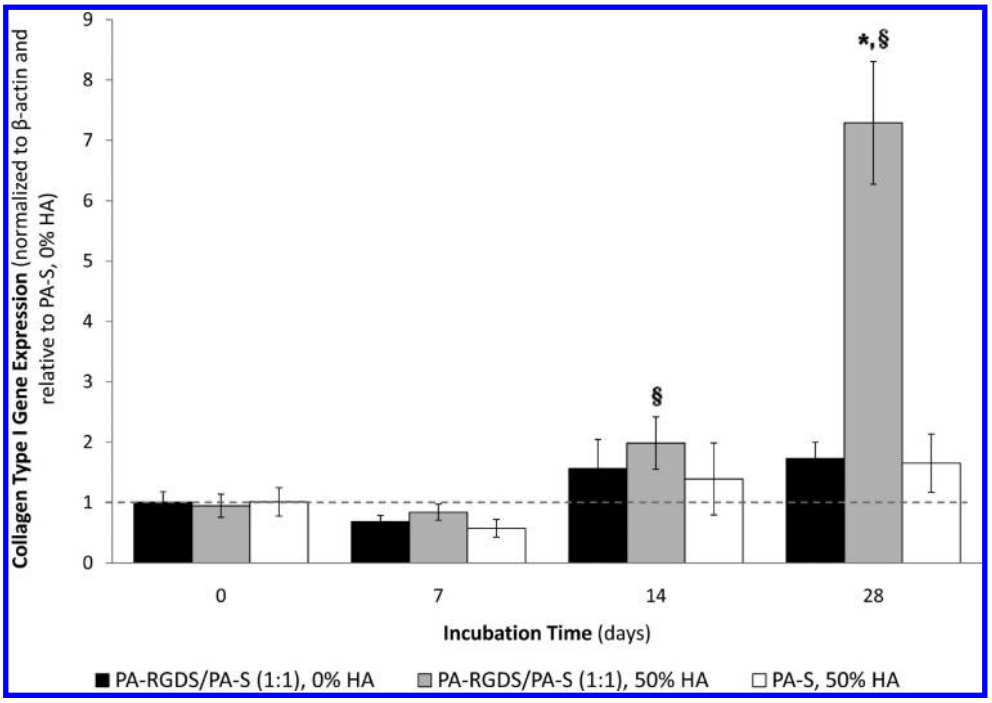

Figure 7. Gene expression profile for collagen type I over 28 days. Values expressed as mean ± standard deviation relative to PA-S, 0% HA (dashed line) for each time point. PA-RGDS/PA-S (1:1), 50% HA promoted significantly greater expression than (*) PA-RGDS/PA-S (1:1), 0% HA and PA-S, 50% HA on Day 28 and (§) normalization control of PA-S, 0% HA ($p < 0.05$).

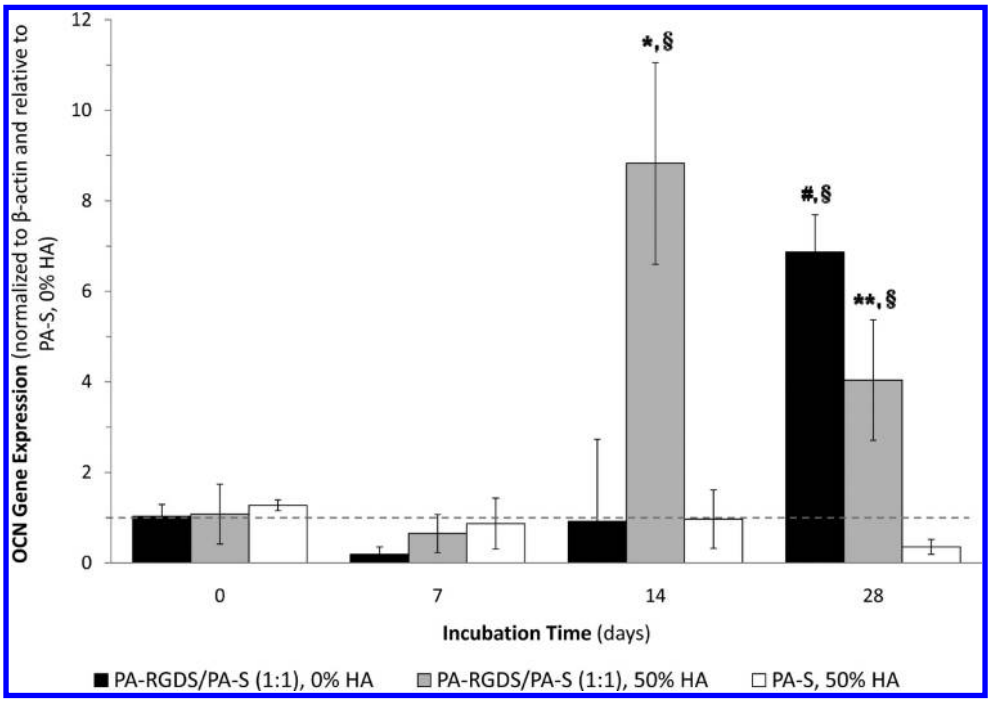

Figure 8. Gene expression profile for OCN over 28 days. Values expressed as mean ± standard deviation relative to PA-S, 0% HA (dashed line) for each time point. PA-RGDS/PA-S (1:1), 50% HA promoted significantly greater expression than (*) PA-RGDS/PA-S (1:1), 0% HA and PA-S, 50% HA on day 14 and (**) PA-S, 50% HA on day 28. (#) PA-RGDS/PA-S (1:1), 0% HA expressed more than PA-RGDS/PA-S (1:1), 50% and PA-S, 50% HA on day 28. (§) Samples greater than the normalization control of PA-S, 0% HA ($p < 0.05$).

implanted PA hydrogels stabilized by intramedullary k-wire supports (Figure 10). It was progressively found that as the PA-RGDS/PA-S (1:1) hydrogel by itself (0% HA) and then biphasic PA-RGDS/PA-S (1:1) containing 50% HA was incorporated, the callus formation across the critical size (6 mm) femoral defect increased, indicating a promoted healing response in the rat model. As a negative control, no PA hydrogel was

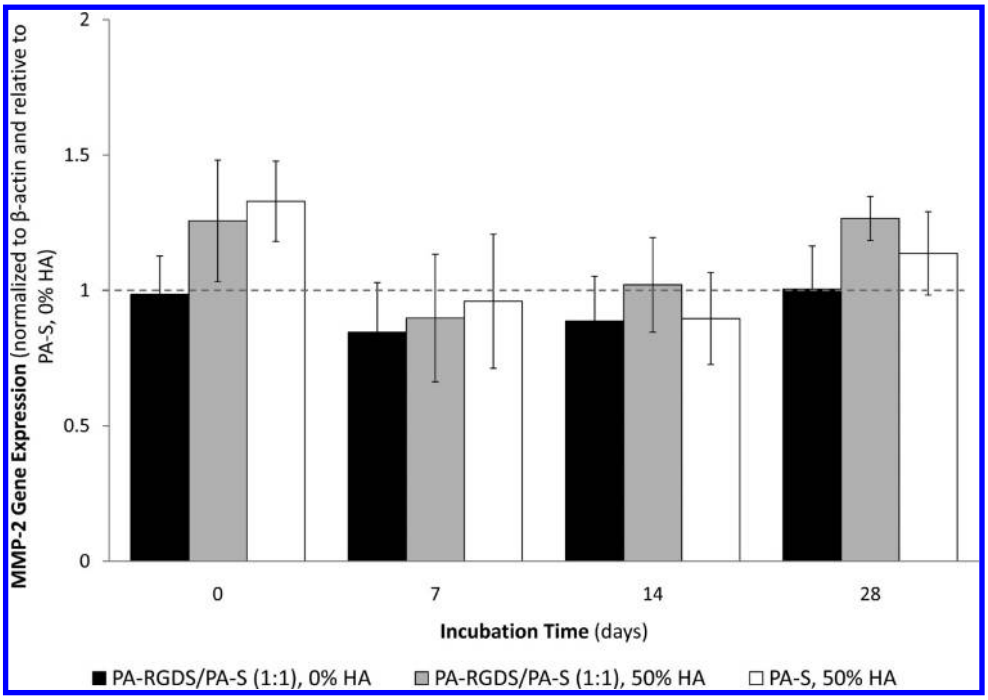

Figure 9. Gene expression profile for MMP-2 over 28 days. Values expressed as mean ± standard deviation relative to PA-S, 0% HA (dashed line) for each time point.

added to the defect site; consequently, the injury defect remained relatively unaffected. However, in the presence of PA-RGDS/PA-S (1:1), 0% HA, there was increased callus formation based on new bone growth after two weeks, resulting in a smaller defect size. The bone healing response was further increased by PA-RGDS/PA-S (1:1), 50% HA, as implantation with the biphasic hydrogel led to new callus formation that bridged the gap across the critical size defect. Furthermore, cortical bone thickening was observed for the biphasic hydrogel condition at the two weeks time point. Observing the healing progression after four weeks, the same general trend was found. While smaller in size, the segmental defect still remained visibly evident for the defect only control. However, the implanted PA-RGDS/PA-S (1:1), 0% HA displayed new callus formation that connected the gap across the defect area, indicating comparatively better new bone growth. For the biphasic PA hydrogel condition, again, a more complete bone healing response was found, as the defect void continued to be filled by new bone formation after initially bridging the segmental gap within the first two weeks.

Histology Assessment. The formation of new bone in the critical size femoral defects was further studied by histological evaluation at the terminal four weeks time point. For all three experimental conditions of the preliminary animal study, a detailed perspective of bone regeneration was provided by Goldner's trichrome staining (Figure 11). Osteoid formation (dark pink staining) was evident across the segmental gaps for all rat femoral defects. However, the biphasic PA-RGDS/PA-S (1:1), 50% HA condition exhibited much more mature bone formation across the defect void, evidenced by the narrower gap and bridging of calcified bone tissue (green staining). Neither of the other conditions demonstrated signs of calcified mineralization across the entire defect, but the PA-RGDS/PA-S (1:1), 0% HA hydrogel condition did show a slightly smaller void of osteoid-stained tissue compared to the defect only control. Thus, the histological evidence, combined with radiography, supports enhanced bone formation promoted by the biphasic PA hydrogel, as evidenced by the pilot animal study.

DISCUSSION

For this study, a bone ECM analogous scaffold was developed and investigated as a tissue engineering solution for stimulated osteoinduction with great promise for long-term bone repair based on preliminary animal model results. This work thereby addresses several of the challenges that lie in the development of synthetic bone tissue engineered materials aimed to recapitulate the fundamental components of natural bone ECM assembly; namely, a multiphase composite needed to capture the organic fibrous structure and inorganic mineralization inherent to native bone tissue formation. Hence, biphasic PA nanomatrix hydrogels were created to address these limitations, providing a bone ECM analogue similar in biological and structural complexity. It was believed that the self-assembling nanofibrous PAs endowed with biological ligand signaling would elicit increased osteoinduction of hMSCs when combined with HA nanoparticles to create a

Figure 10. High resolution radiographs taken after (a−c) two and (d−f) four weeks postoperatively. Representative images shown for (a,d) defect only, (b,e) PA-RGDS/PA-S (1:1) hydrogel, and (c,f) biphasic PA-RGDS/PA-S (1:1), 50% HA. All images taken as lateral radiographs of the 6 mm critical size rat femoral defects.

biphasic scaffold for bone tissue regeneration that could be effectively translated to clinical bone repair. First, different HA concentrations were tested in the PA hydrogels to ensure viscoelastic stability of the biphasic scaffolds as an implantable biomaterial. Then, hMSCs were encapsulated in the self-assembled biphasic PA hydrogels for cellular observation, and the combined influences of functionalized ligand signaling and HA inclusion within the hydrogel scaffolds were studied for osteoinduction efficacy, both *in vitro* and *in vivo*.

Previous literature has shown that the inclusion of HA in combination with bulk polymer biomaterials can be used to directly control and improve upon the physical properties of composite scaffolds.[27,29,47] Many factors must be considered in the evaluation of viscoelastic properties for HA-containing hydrogels, including mineral shape, size, filler volume/weight percentage, molecular weight, and state of interface between mineral and polymer, as all can directly impact the overall gelation quality.[4] As described earlier, both PA-RGDS/PA-S (1:1) and PA-S were first self-assembled into hydrogels and evaluated across a wide range of HA weight concentrations based on dynamic oscillatory rheometry, previously established as an appropriate evaluation criterion for hydrogels.[16,17,48] Additionally, only inorganic HA nanoparticles with a Ca/P ratio of 1.6 were embedded, which approximates the composition found in native bone.[49]

It was found that the 50% HA weight concentration exhibited the greatest viscoelastic response out of all PA conditions tested. In terms of clinical relevance, the 50% HA concentration effectively approximates the ratio found in native bone, as it has been determined that inorganic minerals compose about half of the dry weight of the bone matrix.[50] Furthermore, this result is similar to previous work in which the 50% HA weight ratio produced the best stabilizing physical condition before dropping off at higher HA concentrations.[51] It is believed that the interactions between polymer and HA particles in composite biomaterials, such as the biphasic PA nanomatrix, lead to improved physical properties; specifically, it has been reported that strong interfacial bonding can result between mineral and polymer, effectively transferring the load from the matrix to mineralized reinforcements for better structural durability.[52] Thus, along with displaying stable macroscopic gel quality, the increased viscoelastic response demonstrates an enhanced ability of the biphasic PA nanomatrix hydrogels to store deformation energy that is most effective at the 50% HA concentration compared to the other embedded concentrations. This is vital to clinician handling and long-term stability, as the material is developed for implantation in tissue regeneration applications.[53]

Additionally, the nanostructures of the biphasic PA hydrogels were observed to ensure that PA nanofiber self-assembly was unaffected by the inclusion of HA nanoparticles. For all PA hydrogels, nanofiber self-assembly was induced by charge neutralization using calcium divalent ions under physiological conditions, resulting in ionic bridging of the negatively charged PA molecules. Successful PA nanofiber self-assembly was evident for both biphasic hydrogels tested at the 50% HA concentration. Only TEM images of the biphasic PA hydrogel conditions were included because the single-phase PA (0% HA) hydrogels have been previously verified.[17] Regardless, PA self-assembly was able to successfully embed HA nanoparticles for all conditions. However, little is known about the interactions between PA nanofibers and HA nanoparticles or the forces that hold them together within the biphasic nanomatrix. It has been suggested that HA interacts with PA nanofibers through the calcium ion mediators of gelation, as these ions serve as short-distance bridges to hold together the two biphasic components with support from hydrogen and van der Waals forces.[14,54]

The development of biphasic PA nanomatrix hydrogels with enhanced viscoelastic stability at the 50% HA

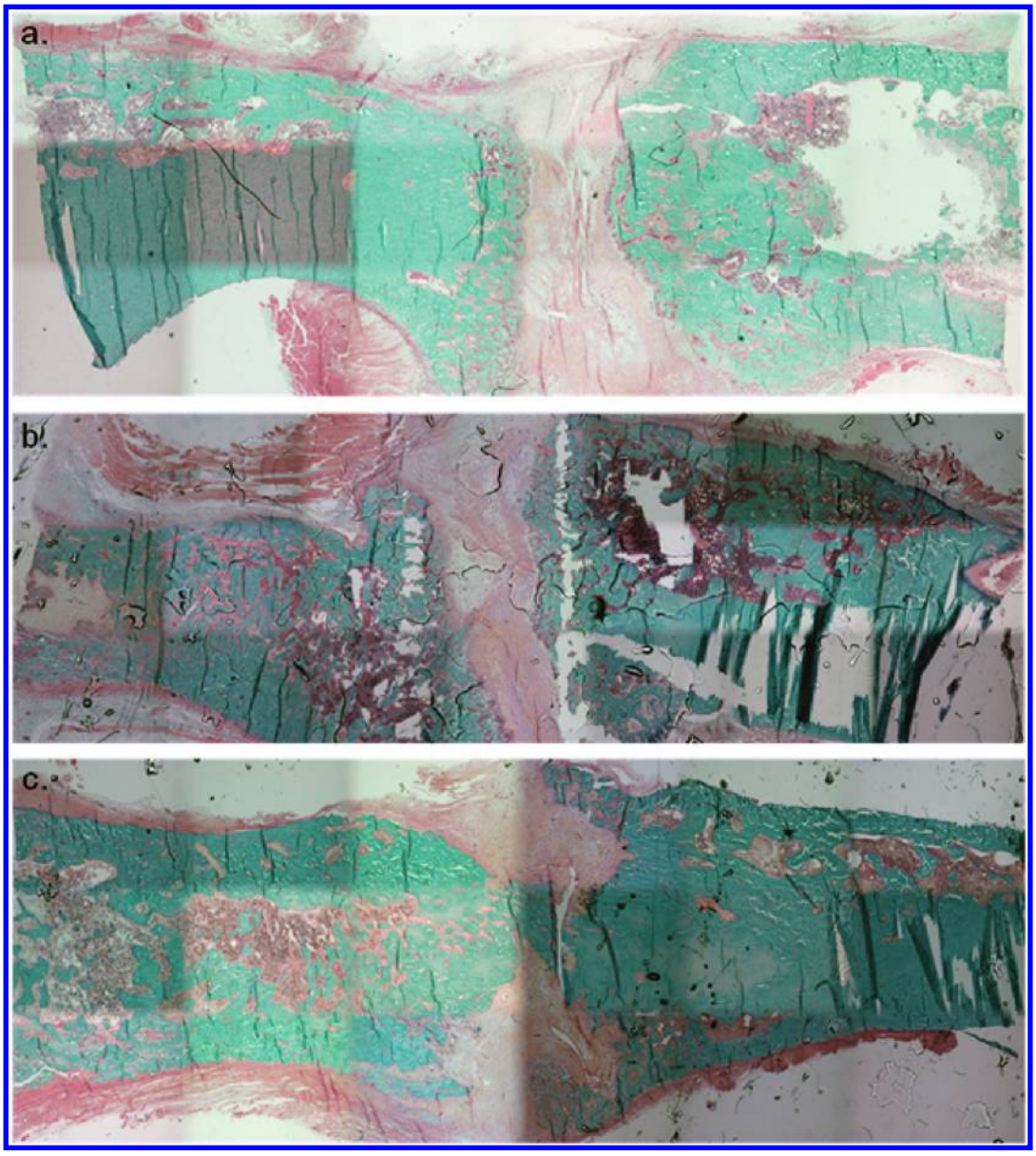

Figure 11. Histological evaluation of 6 mm critical size femoral defects after four weeks using Goldner's trichrome staining. Representative images shown for (a) defect only, (b) PA-RGDS/PA-S (1:1) hydrogel, 0% HA and (c) biphasic PA-RGDS/PA-S (1:1), 50% HA. Osteoid stains dark pink, and calcified bone tissue appears green.

concentration established a composite scaffold ready for biological evaluation. For all cell response studies, the PA hydrogels were seeded with hMSCs and evaluated for up to 28 days *in vitro*. hMSCs were chosen because they are widely regarded as a stem cell for osteoblasts, differentiating along an osteogenic lineage when properly stimulated.[55] Furthermore, hMSCs are locally accessible at the bone microenvironment, being one of the first major cell types recruited to the surface of implanted bone biomaterials.[43,56] Evaluating the PA nanomatrix hydrogels with hMSCs, initial viability was first examined. Positive Live/Dead viability staining confirmed biocompatibility of the encapsulated hMSCs for all PAs hydrogels, both with and without embedded HA nanoparticles. Furthermore, high cell confluency was observed for each condition throughout the three-dimensional hydrogels, which is believed to enable the close cell-to-cell communications needed for long-term cellularity and osteogenic differentiation.[57,58]

Studying the long-term cellularity, it was found that both PA-RGDS/PA-S (1:1) hydrogels, with and without HA, exhibited higher cellular content, especially within the first two weeks, and that the biphasic RGDS-containing (50% HA) gel was more effective between the two. The increase in cellularity with inclusion of HA is supported by past literature investigating HA-polymer composites; in these studies, greater cell adherence and retention is attributed to the high adsorbent properties of HA, leading to enhanced serum protein adsorption and improved overall cellularity.[59,60]

Despite the added benefits of HA, the bioactive signaling of the RGDS ligand within the PA hydrogels is still believed to be the greatest effector of observed cellularity. Besides the established history of RGDS ligand signaling increasing cell adhesion, the results from this study showed that both RGDS-mediated PA nanomatrix hydrogels exhibited greater cellularity compared to PA-S gels, even when HA was included.[61] It should be noted, however, that the observed amounts of hMSCs in the PA hydrogels peaked after the first week, as cellularity was only maintained with minimal proliferation thereafter. This reduction in continued long-term proliferation is partly attributed to the shift in a proliferative to differentiated state of the encapsulated cells as mediated by the osteoinductive scaffold microenvironments, along with cell losses from the required cell culture media changes every 3−4 days of the tissue culture plates supporting the seeded PA hydrogels, thus leading to no net gains in encapsulated cell populations after the first week of incubation. Regardless, all PA scaffolds retained enough cells per hydrogel to meet the minimum cellularity threshold needed to support osteogenic differentiation, enabling long-term evaluation of osteoinduction and *in vivo* bone healing facilitated by the PA nanomatrix hydrogels.[41]

Many different types of scaffolds exist for bone tissue engineering, as comprehensively reviewed in the literature.[28,62] However, the emphasis of this study has been placed on synthetic hydrogel scaffolds, especially composites that incorporate inorganic minerals, such as HA. In this regard, the use of self-assembling peptide-based scaffolds for osteoinduction and applied bone tissue engineering is an emerging area of exploration with many remaining questions still unanswered. Previously, two of the main classes of self-assembling peptide scaffolds investigated include the PuraMatrix and PA biomaterials. PuraMatrix, originally designated as RAD16-I, has exhibited excellent biocompatibility, and studies have shown that the injectable hydrogel can lead to formation of bony bridges and mature tissue healing of bone defects under *in vivo* conditions.[63,64] At the same time, PAs have demonstrated many of the same qualities, while also being developed to nucleate HA crystals from minerals in the surrounding osseous microenvironment onto the nanomatrix itself.[10,65] *In vivo* studies conducted with these HA nucleating PAs have been shown to promote bone formation in rat femoral defects.[66] Thus, this study investigated the effects of HA nanoparticle inclusion from the onset of cellular response, as mineral embedment during initial self-assembly could potentially stimulate the localized hMSCs into an earlier osteogenic phenotype for improved bone healing. On the basis of the quantitative osteogenic gene expression results *in vitro* and preliminary animal model study, there is much promise to this organic/inorganic biphasic approach. The RGDS-mediated biphasic PA containing 50% HA expressed the greatest phenotypic profile for all osteogenic markers evaluated throughout the four week incubation and promoted the best comparative bone healing response of the critical size femoral defect *in vivo*. Additionally, the single-phase PA-RGDS/PA-S (1:1) hydrogel without HA tended to be slightly higher in temporal gene expression than PA-S at both HA conditions, especially in regards to OCN expression, suggesting that the RGDS ligand signaling is a more important factor in osteoinduction than HA nanoparticles within the biphasic composite.

Mechanisms behind the stimulated osteoinductive response of hMSCs are believed to be mediated by both key components of the RGDS-containing biphasic PA nanomatrix hydrogel, as the combined influence of bioactive RGDS ligand signaling from PA nanofibers and embedded HA nanoparticles worked together to create a bone ECM analogous microenvironment. Individually, the RGDS ligand has been found to induce osteogenic differentiation based only on the cell-ligand interactions presented within self-assembling scaffolds.[18,35,36] It is believed that RGDS ligand signaling most likely stimulates osteoinduction through integrin-mediated activation of the ERK-related intracellular pathways.[67] Additionally, previous studies investigating the osteogenic response in HA-containing composite scaffolds have found that the addition of HA increased the observed level of differentiation.[27,33,34] However, little is known of the driving mechanisms involved or what role, if any, that HA plays in the osteoinductive process. Some insight has begun to emerge, though; it has been suggested by Song *et al.* that HA is capable of activating the ERK-related osteoinductive signaling pathway, governing cell response on a molecular level by its presence.[68]

Gene expression was also confirmed for MMP-2 for all PA nanomatrix hydrogels evaluated. No major differences in overall MMP-2 gene expressions were found, and relative expression levels were maintained throughout the entire four weeks *in vitro* cultivation. The unbiased expression of MMP-2 for all PA conditions is important because its presence enables potential cell migration and bioresponsive degradation of the PA nanomatrix networks over time *via* the incorporated enzyme-cleavable sequences.[16] This is necessary for new tissue in-growth and localized ECM maturation, as the biphasic PA nanomatrix hydrogel continues to be developed for bone tissue regeneration.

Lastly, translation of the biphasic PA nanomatrix hydrogel to an *in vivo* critical size bone defect model was investigated as a preliminary study to understand the guided regenerative ability and clinical effectiveness under physiological conditions. The focus was on bone healing potential of the RGDS-mediated PA nanomatrix, with and without inorganic HA nanoparticles, included to create a bone ECM analogous biphasic scaffold. A critical size femoral defect of 6 mm

in a rat animal model was used for *in vivo* evaluation. Three different experimental study groups were tested, consisting of defect only, PA-RGDS/PA-S (1:1) without HA, and the biphasic PA-RGDA/PA-S (1:1) hydrogel with 50% HA, all stabilized by an intramedullary k-wire for load-bearing support. From the observed results, the biphasic PA nanomatrix containing RGDS ligand signaling and inorganic HA nanoparticles demonstrated the best comparative bone healing response based on bridging of bone tissue across the defect void after four weeks. The PA nanomatrix hydrogel without HA followed in regenerative potential, exhibiting a smaller defect void in comparison to the defect only control. Of note, the 6 mm defect gap for the defect only condition remained disjoined throughout the study, confirming the nonhealing nature of the femoral osteotomy at this critical defect size.

The increased bone healing formation in the presence of implanted biphasic PA nanomatrix correlates with other animal model studies that observed an improved healing response through the use of peptide-based, self-assembling hydrogels.[63,64,66] In accordance with the *in vitro* results, it is believed that the improved bone healing response, again, was driven by the two critical mediators in the biphasic PA nanomatrix scaffold. As hMSCs are one of the first cell types recruited to bone injury sites, the accessibility of RGDS ligand signaling within the biphasic PA nanomatrix hydrogel was believed to mediate the osteogenic response of locally present progenitor cells, creating a microenvironment predisposed to osteogenesis and better bone repair. Concurrently, inorganic HA nanoparticles, as embedded within the PA nanomatrix hydrogel, were available from the onset of injury repair at the bone defect site. The early presence of biologically relevant HA offers a readily available mineralization source to potentially increase osteogenic maturation of progenitor cells, enhancing the bone healing response. Therefore, the biphasic composite of bioactive PA nanomatrix embedded with HA nanoparticles demonstrated improved bone healing *in vivo*, providing an analogous bone ECM scaffold as a potential solution for clinically effective tissue regeneration.

As the biphasic PA nanomatrix hydrogel continues to be developed for bone tissue regeneration, future studies are still needed to improve the overall osteoinductive efficacy and clinical regenerative ability. This includes further exploration of the biphasic nanomatrix using different amounts of embedded HA concentrations and more comprehensively evaluating the distribution of nanoparticles within the PA scaffold. More in-depth study of the amounts of initially seeded cells and comparisons to positive controls, such as BMP-2, are intended as well to better understand the effects on long-term osteoinduction. Furthermore, larger scale animal model studies investigating many unexplored questions remain. This includes microcomputer tomography imaging and mechanical testing of the healed bone limbs at terminal end points to provide a more comprehensive assessment of the overall healing response. Also, future *in vivo* studies intend to encapsulate hMSCs within the nanomatrix hydrogels to provide an additional conduit for promoting bone regeneration. By introducing a biological component at the femoral defect sites, the clinical effectiveness of the biphasic nanomatrix hydrogels may increase significantly over the already promising bone healing response.

CONCLUSIONS

Bone ECM analogous synthetic hydrogel scaffolds have been developed for this study, consisting of self-assembling PAs endowed with tissue-specific ligand signaling and interspersed HA nanoparticles. The combination of organic PAs and reinforcing inorganic HA created a biphasic PA nanomatrix, intended to improve hydrogel viscoelasticity, stimulate osteoinduction of encapsulated hMSCs *in vitro*, and promote bone tissue regeneration of a femoral defect *in vivo*. Controllable viscoelasticity of the biphasic PA nanomatrix hydrogels was demonstrated through modulation of embedded HA content, with the 50% HA concentration determined to be most stable for improved durability as an implantable biomaterial. After confirming initial biocompatibility, extended observations of cellular response showed that the RGDS-mediated biphasic PA nanomatrix hydrogel promoted enhanced osteoinduction over the entire progression of phenotypic markers. Lastly, a preliminary animal study was conducted using a critical size femoral defect rat model. The best comparative bone healing response was stimulated by the biphasic PA nanomatrix hydrogel based on radiography and histology. These results provide innovative insights into a promising biomimetic tissue engineering approach, offering one of the first observations of a bone ECM analogue combining both organic and inorganic phases with great potential for clinical effectiveness. Thus, the biphasic PA hydrogel establishes a self-assembling nanomatrix that captures the hierarchical nanostructured formation and biological complexity of native ECM for bone tissue engineering.

MATERIALS AND METHODS

Peptide Amphiphile Synthesis and Characterization. All PA molecules were synthesized by solid-phase peptide synthesis using previously described methods.[16−19,24] Two different PA sequences were prepared, designated as PA-RGDS [$CH_3(CH_2)_{14}$CONH-GTAGLIGQ-RGDS-COOH] and PA-S [$CH_3(CH_2)_{14}$CONH-GTAGLIGQ-S-COOH]. Briefly, standard Fmoc-chemistry was performed on an Advanced Chemtech Apex 396 peptide synthesizer (AAPPTec,

Louisville, KY) for all peptide sequences. Palmitic acid in a solution of *o*-benzotriazole-*N*,*N*,*N*′,*N*′-tetramethyluroniumhexafluorophosphate, diisopropylethylamine, and dimethylformamide was coupled directly to the N-termini of the peptide sequences to add the hydrophobic aliphatic tail. Each PA was then cleaved from the resin using a mixture of trifluoroacetic acid (TFA), deionized (DI) water, triisopropylsilane, and anisole (40:1:1:1). After cleavage, each PA underwent rotoevaporation to remove excess TFA and was precipitated in cold diethyl ether. The collected precipitates were dried by lyophilization for 3 days, and the final PA products were analyzed for impurities by matrix-assisted laser desorption ionization time-of-flight (MALDI-TOF) mass spectrometry.

Self-Assembly Formation of Biphasic Peptide Amphiphile Nanomatrix Hydrogels. PAs were first dissolved in DI water to create 2% (weight/volume) stock solutions and buffered to neutral pH (~7) with NaOH. For gelation stability, PA-RGDS was mixed with PA-S at a molar ratio ($Mr_{PA\text{-}S}$ = PA-RGDS/PA-S) of 1:1, as previously described.[17] Hence, all experiments investigating the RGDS-containing PA hydrogel have been denoted as PA-RGDS/PA-S (1:1). To create the biphasic PA hydrogels, HA nanoparticles (Berkeley Advanced Biomaterials Inc., CA) with a Ca/P ratio of 1.6 were embedded in the PA stock solutions. The HA nanoparticles were in the form of needle-shaped dry powder granules with purity of 90% and average particle size of 100 nm, as previously characterized.[69−71] Self-assembly of the biphasic PA hydrogels was induced by combining the PA/HA mixtures with $CaCl_2$ (0.1 M) and cell culture medium in 12-well silicone flexiPERM cell-culture chambers attached to glass coverslips. The molar ratio between PAs and calcium ions ($Mr_{Ca} = Ca^{2+}/PA$) was held constant at $Mr_{Ca} = 2$ for all cases. Testing a wide range of HA content, the HA concentrations evaluated in the biphasic PA hydrogels included 0%, 33%, 50%, and 66.7% (% = HA mass/total mass). The HA concentration percentage values have been designated at the end of PA data labels for all experiments.

Characterization of Gelation and Nanofiber Self-Assembly Properties. After inducing self-assembly with embedded HA, the gelation properties of the biphasic PA nanomatrix hydrogels were studied. Viscoelasticity was rheologically characterized on an AR 2000 Rheometer (TA Instruments, UK), as described previously.[17] For each characterization, the storage modulus (G') and loss modulus (G'') were measured across a wide frequency range (0.1−10 Hz) at 25 °C. Furthermore, the effect of HA inclusion on PA nanofiber self-assembly was evaluated by transmission electron microscope (TEM), using previously described methods.[16,17,72] Accompanying macroscopic images of the biphasic PA gels were also taken to provide overall views of the gelation character and stability.

Cell Culturing in Biphasic Peptide Amphiphile Nanomatrix Hydrogels. Based on viscoelastic stability, the HA concentration was fixed at 50% HA for all biphasic PA nanomatrix hydrogels, while the other self-assembly parameters remained the same. Human mesenchymal stem cells (hMSCs) (Lonza, Walkersville, MD) isolated from bone marrow were used for all cell culturing experiments. Cells were grown in normal cell culture medium prior to encapsulation within the PA hydrogels. Normal cell culture medium consisted of Dulbecco's Modified Eagle's Medium (DMEM) (Mediatech, Manassas, VA), 10% fetal bovine serum (FBS) (Atlanta Biologicals, Lawrenceville, GA), 1% Amphotericin B, 1% penicillin, and 1% streptomycin (Mediatech). Cells were only seeded within a passage number of 3−6. Before cell encapsulation, the tissue culture plates and well inserts, aliquoted HA, and PA stock solutions were UV sterilized for at least 4 h. Afterward, hMSCs were lifted with 0.05% trypsin/EDTA solution and resuspended in normal culture medium at a concentration of 5 000 000 cells/mL. The biphasic PA hydrogels were then self-assembled with embedded HA as described earlier, except hMSCs were present in the cell culture medium during gelation. Specifically, a cell suspension of 10 μL (50000 cells/hydrogel) was encapsulated into each PA hydrogel in combination with $CaCl_2$ (0.1 M) during self-assembly induction. After self-assembly, cell encapsulated PA hydrogels were transferred to cell culture well inserts (0.4 μm pore size) in 24-well tissue culture plates (BD Biosciences, CA) for long-term *in vitro* incubation. Osteogenic supplements were added to the cell culture medium, consisting of 100 nM dexamethasone, 10 mM β-glycerol phosphate, and 0.05 mg/mL ascorbic acid (Sigma Aldrich, St. Louis, MO), based on previously documented formulations.[73,74] Cell cultures were maintained under standard conditions (37 °C, 95% relative humidity, 5% CO_2) with media changes every 3−4 days. Samples were collected after 0, 7, 14, and 28 days using similarly described methods and stored at −80 °C before biochemical analyses.[18,19]

Cellular Viability Staining. Initial viability of encapsulated hMSCs in the PA nanomatrix hydrogels was qualitatively observed under fluorescent microscopy using the Live/Dead Viability/Cytotoxicity Kit (Invitrogen) per manufacturer instructions. Briefly, after 3 days cultivation, cell culture medium was removed from each PA hydrogel sample *via* manual aspiration. Live/Dead solution containing calcein AM and ethidium homodimer-1 was added and incubated for 30 min at 37 °C to fluorescently stain all samples. After incubation, the Live/Dead solution was removed and replaced with PBS for sample hydration during imaging. Cellular viability was visualized under a Zeiss LSM 710 confocal laser scanning microscope (Thornwood, NY).

Measurement of Cellularity. The cellularity for all samples was measured using the PicoGreen assay kit (Molecular Probes, Eugene, OR), quantifying the amount of double-stranded DNA content at each time point according to the manufacturer instructions. Briefly, the collected samples were removed from −80 °C storage and subjected to a thaw/freeze cycle (30 min thawing at room temperature, 15 min sonication, freezing at −80 °C for 1 h) to lyse the cells. PicoGreen dye was then added for fluorometric quantification of DNA content, and the concentration was measured using a fluorescent microplate reader (Synergy HT, BIO-TEK Instruments, Winooski, VT) filtered at 485/528 (EX/EM).

Gene Expression Using Quantitative Real-Time Polymerase Chain Reaction. RNA extraction was performed using the TRIzol reagent (Invitrogen, Carlsbad, CA) for all samples based on manufacturer instructions. After total RNA collection, the samples were centrifuged into pellets, dried, and resuspended in nuclease-free water. DNase treatment (TURBO DNase, Ambion, Austin, TX) was performed to prevent any residual genomic DNA contamination, followed by measurement of RNA concentrations using a ND-1000 UV spectrophotometer (Nanodrop, Wilmington, DE). Based on 1 μg per sample, each RNA sample was reversed-transcribed into cDNA using the iScript cDNA Synthesis kit (Bio-Rad, Hercules, CA), as instructed by the manufacturer. For real-time PCR detection, the iQ SYBR Green Supermix (Bio-Rad) was used for quantification on an iCycler iQ Real-Time PCR machine (Bio-Rad). The PCR amplification conditions were 95 °C for 3 min, followed by 40 cycles of 95 °C for 20 s, 55 °C for 20 s, and 72 °C for 20 s. Specific primer sequences for Runx2, alkaline phosphatase (ALP), collagen type I, osteocalcin (OCN), matrix metalloproteinase-2 (MMP-2), and β-actin (housekeeping gene) were used to evaluate gene expression, as listed in Table 2. Negative control samples without the cDNA template were run concurrently to check for genomic DNA contamination. All gene expression data were normalized to the internal standard of β-actin and calculated using the $2^{-\Delta\Delta Ct}$ method, previously described.[75] Hence, differences in gene expression have been expressed as the fold ratio relative to the PA-S, 0% HA control group after β-actin normalization for each time point.

Surgical Implantation and Retrieval. All procedures involving animals were in compliance with the guiding principles of the "Care and Use of Animals" and approved by the University of Alabama at Birmingham Institutional Animal Care and Use Committee (IACUC). For scaffold implantation, 8−10 weeks-old male athymic rats were anesthetized with isoflurane administered *via* an inhalation chamber. A single hindlimb per each rat was shaved and prepared for surgery. The femoral defect size of 6 mm was then created under sterile conditions. Briefly, the femur was approached anterolaterally by incising the periosteum and then elevating circumferentially along the entire femur. The full thickness defect (6 mm) was created in the diaphysis using a circular saw. The bone was stabilized with internal fixation using an intramedullary threaded k-wire. After

TABLE 2. Primer Sequences for Real-Time PCR

primer	sequence (5′−3′)	GenBank identification
β-actin		NM_001101
sense	CGT CTT CCC CTC CAT CGT	
antisense	GAA GGT GTG GTG CCA GAT TT	
Runx2		NM_004348
sense	AGA TGA TGA CAC TGC CAC CTC TG	
antisense	GGG ATG AAA TGC TTG GGA ACT	
alkaline phosphatase (ALP)		NM_000478
sense	ACC ATT CCC ACG TCT TCA CAT TT	
antisense	AGA CAT TCT CTC GTT CAC CGC C	
collagen type I		NM_000088
sense	AGT TGG TGC TAA GGG TGA AG	
antisense	GCA ATA CCA GGA GCA CCA	
osteocalcin (OCN)		NM_199173
sense	CAA AGG TGC AGC CTT TGT GTC	
antisense	TCA CAG TCC GGA TTG AGC TCA	
matrix metalloproteinase-2 (MMP-2)		NM_004530
sense	GGC CTC TCC TGA CAT TGA CC	
antisense	TCA CAG TCC GCC AAA TGA AC	

controlling the bleeding, each PA hydrogel was individually implanted into the defect site prior to wound closure. Three samples for each experimental group (defect only, PA-RGDS/PA-S, 0% HA only, biphasic PA-RGDS/PA-S, 50% HA) were implanted. The amounts of PA-RGDS, PA-S, HA, and calcium ions were adjusted as needed to fully fill the defect void, while still maintaining the fixed scaffold design ratios. After implantation, the muscle cuff and overlapping skin were sutured closed. Postoperatively, buprenorphine was administered every 8 h for 3 days for pain management, and the animals were allowed to walk freely. The animals were monitored every other day for signs of infection or other abnormalities. After 4 weeks, the animals were sacrificed *via* exsanguinations. The femur specimens with implanted scaffolds were then retrieved for histology assessment.

Radiographic Analysis. High resolution radiographs of the femoral defects (6 mm) in athymic rats were taken *in vivo*. Radiographic imaging was carried out by the Small Animal Bone Phenotyping Core at the University of Alabama at Birmingham to provide noninvasive assessment of new bone growth. For radiography, the rats were anesthetized with isoflurane and laid on the imaging plate in a prostrate position. Each femur was positioned laterally in the X-ray machine and imaged with maximum visualization of the defect. Radiography was performed with a Faxitron model MX-20 tabletop X-ray machine (Wheeling, Illinois) and processed as digital X-rays randomly selected as representative images for the 2 and 4 weeks time points.

Histology Assessment. Bone histology was performed by the Histomorphometry and Molecular Analyses Core at the University of Alabama at Birmingham. After animal sacrifice at 4 weeks, the internal fixators were removed from all collected femurs, and the specimens preserved in 10% formalin solution. The femur specimens were then randomly selected for embedment in polymethylmethacrylate (cut at 5 μm on Leica 2265 microtome) for Goldner's trichrome staining. The tissue sections were deplasticized in 60 °C xylene overnight, followed by hydration in graded alcohols. The sections were then stained with Weigert−Hematoxylin for 30 min, followed by Ponceau/fuchsin solution for 15 min, rinsed in 1% acetic acid for 1 min, and stained with phosphomolybdic acid-orange G solution for 15 min. The sections were rinsed again in 1% acetic acid for 1 min and counterstained with light green for 15 min. Finally, the sections were dehydrated, cleared, and mounted. From the Goldner's trichrome staining, osteoid regions show as dark pink, and calcified bone appears green.

Statistical Analysis. All quantitative experiments were performed three independent times. Representative graphical results performed at least in triplicate are each expressed as mean ± standard deviation. All statistical analyses were performed using SPSS 15.0 software (SPSS Inc., IL). One-way analysis of variance (ANOVA) was used for statistical comparison, with differences between pairs determined by the Tukey multiple comparisons test. A value of $p < 0.05$ was considered statistically significant.

Acknowledgment. The authors gratefully acknowledge the support of the Mass Spectrometry/Proteomics Shared Facility for analyzing all PA samples and Dr. Derrick Dean for access to rheometry equipment. All TEM and confocal microscopy was conducted with the helpful assistance of Melissa Chimento and Shawn Williams through the High Resolution Imaging Facility. Special thanks are extended to Dr. Ralph Sanderson for use of real-time PCR laboratory facilities, along with Dr. Vishnu Ramani and Dr. Anurag Purushothaman for assistance with all PCR experiments. Additionally, all animal studies were made possible under the guidance and expertise of Dr. Shawn Gilbert and Jessica Goldstein. The Small Animal Bone Phenotyping Core guided by Xingsheng Li and Histomorphometry and Molecular Analyses Core operated by Patricia Lott are gratefully acknowledged for all postoperative animal evaluations. This work was supported by the Wallace H. Coulter Foundation (H.-W.J.), 2010 Intramural Pilot and Feasibility Research Grant from the BioMatrix Engineering and Regenerative Medicine Center at UAB (H.-W.J.), National Science Foundation CAREER Award under Grant Number CBET-0952974 (H.-W.J), and Ruth L. Kirschstein National Research Service Award Individual Fellowship (F31DE021286) from the National Institute of Dental & Craniofacial Research (J.M.A).

REFERENCES AND NOTES

1. Rosso, F.; Giordano, A.; Barbarisi, M.; Barbarisi, A. From Cell-ECM Interactions to Tissue Engineering. *J. Cell. Physiol.* **2004**, *199*, 174–180.
2. Streuli, C. Extracellular Matrix Remodelling and Cellular Differentiation. *Curr. Opin. Cell Biol.* **1999**, *11*, 634–640.
3. Rho, J.-Y.; Kuhn-Spearing, L.; Zioupos, P. Mechanical Properties and the Hierarchical Structure of Bone. *Med. Eng. Phys.* **1998**, *20*, 92–102.
4. Supova, M. Problem of Hydroxyapatite Dispersion in Polymer Matrices: A Review. *J. Mater. Sci.: Mater. Med.* **2009**, *20*, 1201–1213.
5. Benoit, D. S.; Durney, A. R.; Anseth, K. S. The Effect of Heparin-Functionalized PEG Hydrogels on Three-Dimensional Human Mesenchymal Stem Cell Osteogenic Differentiation. *Biomaterials* **2007**, *28*, 66–77.

6. Kim, J.; Hefferan, T. E.; Yaszemski, M. J.; Lu, L. Potential of Hydrogels Based on Poly(Ethylene Glycol) and Sebacic Acid as Orthopedic Tissue Engineering Scaffolds. *Tissue Eng., Part A* **2009**, *15*, 2299–2307.
7. Song, J.; Malathong, V.; Bertozzi, C. R. Mineralization of Synthetic Polymer Scaffolds: A Bottom-up Approach for the Development of Artificial Bone. *J. Am. Chem. Soc.* **2005**, *127*, 3366–3372.
8. Temenoff, J. S.; Park, H.; Jabbari, E.; Sheffield, T. L.; LeBaron, R. G.; Ambrose, C. G.; Mikos, A. G. *In Vitro* Osteogenic Differentiation of Marrow Stromal Cells Encapsulated in Biodegradable Hydrogels. *J. Biomed. Mater. Res., Part A* **2004**, *70*, 235–244.
9. Semino, C. E. Self-Assembling Peptides: From Bio-Inspired Materials to Bone Regeneration. *J. Dent. Res.* **2008**, *87*, 606–616.
10. Hartgerink, J. D.; Beniash, E.; Stupp, S. I. Self-Assembly and Mineralization of Peptide-Amphiphile Nanofibers. *Science (Washington, DC)* **2001**, *294*, 1684–1688.
11. Hartgerink, J. D.; Beniash, E.; Stupp, S. I.; Peptide-Amphiphile Nanofibers, A Versatile Scaffold for the Preparation of Self-Assembling Materials. *Proc. Natl. Acad. Sci. U.S.A.* **2002**, *99*, 5133–5138.
12. Jun, H. W.; Paramonov, S. E.; Hartgerink, J. D. Biomimetic Self-Assembled Nanofibers. *Soft Matter* **2006**, *2*, 177–181.
13. Tovar, J. D.; Claussen, R. C.; Stupp, S. I. Probing the Interior of Peptide Amphiphile Supramolecular Aggregates. *J. Am. Chem. Soc.* **2005**, *127*, 7337–7345.
14. Palmer, L. C.; Newcomb, C. J.; Kaltz, S. R.; Spoerke, E. D.; Stupp, S. I. Biomimetic Systems for Hydroxyapatite Mineralization Inspired by Bone and Enamel. *Chem. Rev. (Washington, DC)* **2008**, *108*, 4754–4783.
15. Beniash, E.; Hartgerink, J. D.; Storrie, H.; Stendahl, J. C.; Stupp, S. I. Self-Assembling Peptide Amphiphile Nanofiber Matrices for Cell Entrapment. *Acta Biomater.* **2005**, *1*, 387–397.
16. Jun, H.-W.; Yuwono, V.; Paramonov, S. E.; Hartgerink, J. D. Enzyme-Mediated Degradation of Peptide-Amphiphile Nanofiber Networks. *Adv. Mater. (Weinheim, Ger.)* **2005**, *17*, 2612–2617.
17. Anderson, J. M.; Andukuri, A.; Lim, D. J.; Jun, H. W. Modulating the Gelation Properties of Self-Assembling Peptide Amphiphiles. *ACS Nano* **2009**, *3*, 3447–3454.
18. Anderson, J. M.; Kushwaha, M.; Tambralli, A.; Bellis, S. L.; Camata, R. P.; Jun, H. W. Osteogenic Differentiation of Human Mesenchymal Stem Cells Directed by Extracellular Matrix-Mimicking Ligands in a Biomimetic Self-Assembled Peptide Amphiphile Nanomatrix. *Biomacromolecules* **2009**, *10*, 2935–2944.
19. Anderson, J. M.; Vines, J. B.; Patterson, J. L.; Chen, H.; Javed, A.; Jun, H. W. Osteogenic Differentiation of Human Mesenchymal Stem Cells Synergistically Enhanced by Biomimetic Peptide Amphiphiles Combined with Conditioned Medium. *Acta Biomater.* **2011**, *7*, 675–682.
20. Andukuri, A.; Kushwaha, M.; Tambralli, A.; Anderson, J. M.; Dean, D. R.; Berry, J. L.; Sohn, Y. D.; Yoon, Y. S.; Brott, B. C.; Jun, H. W. A Hybrid Biomimetic Nanomatrix Composed of Electrospun Polycaprolactone and Bioactive Peptide Amphiphiles for Cardiovascular Implants. *Acta Biomater.* **2011**, *7*, 225–233.
21. Andukuri, A.; Minor, W. P.; Kushwaha, M.; Anderson, J. M.; Jun, H. W. Effect of Endothelium Mimicking Self-Assembled Nanomatrices on Cell Adhesion and Spreading of Human Endothelial Cells and Smooth Muscle Cells. *Nanomedicine* **2010**, *6*, 289–297.
22. Kim, J. K.; Anderson, J.; Jun, H. W.; Repka, M. A.; Jo, S. Self-Assembling Peptide Amphiphile-Based Nanofiber Gel for Bioresponsive Cisplatin Delivery. *Mol. Pharm.* **2009**, *6*, 978–985.
23. Kushwaha, M.; Anderson, J. M.; Bosworth, C. A.; Andukuri, A.; Minor, W. P.; Lancaster, J. R., Jr; Anderson, P. G.; Brott, B. C.; Jun, H. W. A Nitric Oxide Releasing, Self Assembled Peptide Amphiphile Matrix That Mimics Native Endothelium for Coating Implantable Cardiovascular Devices. *Biomaterials* **2010**, *31*, 1502–1508.
24. Lim, D. J.; Antipenko, S. V.; Anderson, J. M.; Jaimes, K. F.; Viera, L.; Stephen, B. R.; Bryant, S. M.; Yancey, B. D.; Hughes, K. J.; Cui, W.; *et al*. Enhanced Rat Islet Function and Survival *in Vitro* Using a Biomimetic Self-Assembled Nanomatrix Gel. *Tissue Eng., Part A* **2011**, *17*, 399–406.
25. Tambralli, A.; Blakeney, B.; Anderson, J.; Kushwaha, M.; Andukuri, A.; Dean, D.; Jun, H. W. A Hybrid Biomimetic Scaffold Composed of Electrospun Polycaprolactone Nanofibers and Self-Assembled Peptide Amphiphile Nanofibers. *Biofabrication* **2009**, *1*, 025001.
26. Vallet-Regí, M.; González-Calbet, J. M. Calcium Phosphates as Substitution of Bone Tissues. *Prog. Solid State Chem.* **2004**, *32*, 1–31.
27. He, J.; Genetos, D. C.; Leach, J. K. Osteogenesis and Trophic Factor Secretion Are Influenced by the Composition of Hydroxyapatite/ Poly(Lactide-*co*-Glycolide) Composite Scaffolds. *Tissue Eng., Part A* **2009**.
28. Hutmacher, D. W.; Schantz, J. T.; Lam, C. X.; Tan, K. C.; Lim, T. C. State of the Art and Future Directions of Scaffold-Based Bone Engineering from a Biomaterials Perspective. *J. Tissue Eng. Regen. Med.* **2007**, *1*, 245–260.
29. Paxton, J. Z.; Donnelly, K.; Keatch, R. P.; Baar, K. Engineering the Bone-Ligament Interface Using Polyethylene Glycol Diacrylate Incorporated with Hydroxyapatite. *Tissue Eng., Part A* **2009**, *15*, 1201–1209.
30. Tampieri, A.; Celotti, G.; Landi, E. From Biomimetic Apatites to Biologically Inspired Composites. *Anal. Bioanal. Chem.* **2005**, *381*, 568–576.
31. Lawson, A. C.; Czernuszka, J. T. Collagen–Calcium Phosphate Composites. *Proc. Inst. Mech. Eng. Part H: J. Eng. Med.* **1998**, *212*, 413–425.
32. Kang, S. W.; Lee, J. S.; Park, M. S.; Park, J. H.; Kim, B. S. Enhancement of *in Vivo* Bone Regeneration Efficacy of Human Mesenchymal Stem Cells. *J. Microbiol. Biotechnol.* **2008**, *18*, 975–982.
33. Muller, P.; Bulnheim, U.; Diener, A.; Luthen, F.; Teller, M.; Klinkenberg, E. D.; Neumann, H. G.; Nebe, B.; Liebold, A.; Steinhoff, G.; *et al*. Calcium Phosphate Surfaces Promote Osteogenic Differentiation of Mesenchymal Stem Cells. *J. Cell. Mol. Med.* **2008**, *12*, 281–291.
34. Xie, J.; Baumann, M. J.; McCabe, L. R. Osteoblasts Respond to Hydroxyapatite Surfaces with Immediate Changes in Gene Expression. *J. Biomed. Mater. Res., Part A* **2004**, *71*, 108–117.
35. Hosseinkhani, H.; Hosseinkhani, M.; Tian, F.; Kobayashi, H.; Tabata, Y. Osteogenic Differentiation of Mesenchymal Stem Cells in Self-Assembled Peptide–Amphiphile Nanofibers. *Biomaterials* **2006**, *27*, 4079–4086.
36. Shin, H.; Temenoff, J. S.; Bowden, G. C.; Zygourakis, K.; Farach-Carson, M. C.; Yaszemski, M. J.; Mikos, A. G. Osteogenic Differentiation of Rat Bone Marrow Stromal Cells Cultured on Arg-Gly-Asp Modified Hydrogels without Dexamethasone and Beta-Glycerol Phosphate. *Biomaterials* **2005**, *26*, 3645–3654.
37. Yang, F.; Williams, C. G.; Wang, D. A.; Lee, H.; Manson, P. N.; Elisseeff, J. The Effect of Incorporating RGD Adhesive Peptide in Polyethylene Glycol Diacrylate Hydrogel on Osteogenesis of Bone Marrow Stromal Cells. *Biomaterials* **2005**, *26*, 5991–5998.
38. Meyers, M. A.; Chawla, K. K. *Mechanical Behavior of Materials*; Prentice Hall: Englewood Cliffs, NJ, 1998.
39. Mezger, T. G. *The Rheology Handbook: For Users of Rotational and Oscillatory Rheometers*, 2nd ed.; Vincentz Network: Hanover, Germany, 2006.
40. Kulterer, B.; Friedl, G.; Jandrositz, A.; Sanchez-Cabo, F.; Prokesch, A.; Paar, C.; Scheideler, M.; Windhager, R.; Preisegger, K. H.; Trajanoski, Z. Gene Expression Profiling of Human Mesenchymal Stem Cells Derived from Bone Marrow During Expansion and Osteoblast Differentiation. *BMC Genomics* **2007**, *8*, 70.
41. Harbers, G. M.; Healy, K. E. The Effect of Ligand Type and Density on Osteoblast Adhesion, Proliferation, and Matrix Mineralization. *J. Biomed. Mater. Res., Part A* **2005**, *75*, 855–869.
42. Mygind, T.; Stiehler, M.; Baatrup, A.; Li, H.; Zou, X.; Flyvbjerg, A.; Kassem, M.; Bunger, C. Mesenchymal Stem Cell Ingrowth and Differentiation on Coralline Hydroxyapatite Scaffolds. *Biomaterials* **2007**, *28*, 1036–1047.

43. Pittenger, M. F.; Mackay, A. M.; Beck, S. C.; Jaiswal, R. K.; Douglas, R.; Mosca, J. D.; Moorman, M. A.; Simonetti, D. W.; Craig, S.; Marshak, D. R. Multilineage Potential of Adult Human Mesenchymal Stem Cells. *Science (Washington, DC)* **1999**, *284*, 143–147.
44. Allori, A. C.; Sailon, A. M.; Warren, S. M. Biological Basis of Bone Formation, Remodeling, and Repair-Part II: Extracellular Matrix. *Tissue Eng., Part B Rev.* **2008**, *14*, 275–283.
45. Lian, J. B.; Stein, G. S. Development of the Osteoblast Phenotype: Molecular Mechanisms Mediating Osteoblast Growth and Differentiation. *Iowa Orthop. J.* **1995**, *15*, 118–140.
46. Stefanidakis, M.; Koivunen, E. Cell-Surface Association between Matrix Metalloproteinases and Integrins: Role of the Complexes in Leukocyte Migration and Cancer Progression. *Blood* **2006**, *108*, 1441–1450.
47. Ishikawa, Y.; Komotori, J.; Senna, M. Properties of Hydroxyapatite−Hyaluronic Acid Nano-Composite Sol and Its Interaction with Natural Bones and Collagen Fibers. *Curr. Nanosci.* **2006**, *2*, 191–196.
48. Nowak, A. P.; Breedveld, V.; Pakstis, L.; Ozbas, B.; Pine, D. J.; Pochan, D.; Deming, T. J. Rapidly Recovering Hydrogel Scaffolds from Self-Assembling Diblock Copolypeptide Amphiphiles. *Nature* **2002**, *417*, 424–428.
49. Hing, K. A. Bone Repair in the 21st Century: Biology, Chemistry or Engineering? *Philos. Trans. A Math. Phys. Eng. Sci.* **2004**, *362*, 2821–2850.
50. Junqueira, L. C. U; Cameiro, J. *Basic Histology: Text & Atlas.*, 10th ed.; Lange Medical Books, McGraw-Hill, Medical Publishing Division : New York, 2003; p 144.
51. Wei, G.; Ma, P. X. Structure and Properties of Nano-hydroxyapatite/Polymer Composite Scaffolds for Bone Tissue Engineering. *Biomaterials* **2004**, *25*, 4749–4757.
52. Bhowmik, R.; Katti, K. S.; Katti, D. R. Influence of Mineral on the Load Deformation Behavior of Polymer in Hydroxyapatite−Polyacrylic Acid Nanocomposite Biomaterials: A Steered Molecular Dynamics Study. *J. Nanosci. Nanotechnol.* **2008**, *8*, 2075–2084.
53. Rehfeldt, F.; Engler, A. J.; Eckhardt, A.; Ahmed, F.; Discher, D. E. Cell Responses to the Mechanochemical Microenvironment−Implications for Regenerative Medicine and Drug Delivery. *Adv. Drug Delivery Rev.* **2007**, *59*, 1329–1339.
54. Sanchez, C.; Julian, B.; Belleville, P.; Popall, M. Applications of Hybrid Organic−Inorganic Nanocomposites. *J. Mater. Chem.* **2005**, *15*, 3559–3592.
55. Gregory, C. A.; Prockop, D. J.; Spees, J. L. Non-hematopoietic Bone Marrow Stem Cells: Molecular Control of Expansion and Differentiation. *Exp. Cell Res.* **2005**, *306*, 330–335.
56. Conget, P. A.; Minguell, J. J. Phenotypical and Functional Properties of Human Bone Marrow Mesenchymal Progenitor Cells. *J. Cell. Physiol.* **1999**, *181*, 67–73.
57. Civitelli, R. Cell−Cell Communication in the Osteoblast/Osteocyte Lineage. *Arch. Biochem. Biophys.* **2008**, *473*, 188–192.
58. Stains, J. P.; Civitelli, R. Cell-to-Cell Interactions in Bone. *Biochem. Biophys. Res. Commun.* **2005**, *328*, 721–727.
59. Matsumura, K.; Hayami, T.; Hyon, S. H.; Tsutsumi, S. Control of Proliferation and Differentiation of Osteoblasts on Apatite-Coated Poly(Vinyl Alcohol) Hydrogel as an Artificial Articular Cartilage Material. *J. Biomed. Mater. Res., Part A* **2010**, *92*, 1225–1232.
60. Zhao, F.; Grayson, W. L.; Ma, T.; Bunnell, B.; Lu, W. W. Effects of Hydroxyapatite in 3-D Chitosan-Gelatin Polymer Network on Human Mesenchymal Stem Cell Construct Development. *Biomaterials* **2006**, *27*, 1859–1867.
61. Hersel, U.; Dahmen, C.; Kessler, H. RGD Modified Polymers: Biomaterials for Stimulated Cell Adhesion and Beyond. *Biomaterials* **2003**, *24*, 4385–4415.
62. Cowan, C. M.; Soo, C.; Ting, K.; Wu, B. Evolving Concepts in Bone Tissue Engineering. *Curr. Top. Dev. Biol.* **2005**, *66*, 239–285.
63. Misawa, H.; Kobayashi, N.; Soto-Gutierrez, A.; Chen, Y.; Yoshida, A.; Rivas-Carrillo, J. D.; Navarro-Alvarez, N.; Tanaka, K.; Miki, A.; Takei, J.; *et al*. Puramatrix Facilitates Bone Regeneration in Bone Defects of Calvaria in Mice. *Cell Transplant.* **2006**, *15*, 903–910.
64. Yoshimi, R.; Yamada, Y.; Ito, K.; Nakamura, S.; Abe, A.; Nagasaka, T.; Okabe, K.; Kohgo, T.; Baba, S.; Ueda, M. Self-Assembling Peptide Nanofiber Scaffolds, Platelet-rich Plasma, and Mesenchymal Stem Cells for Injectable Bone Regeneration with Tissue Engineering. *J. Craniofac. Surg.* **2009**, *20*, 1523–1530.
65. Spoerke, E. D.; Anthony, S. G.; Stupp, S. I. Enzyme Directed Templating of Artificial Bone Mineral. *Adv. Mater. (Weinheim, Ger.)* **2009**, *21*, 425–430.
66. Mata, A.; Geng, Y.; Henrikson, K. J.; Aparicio, C.; Stock, S. R.; Satcher, R. L.; Stupp, S. I. Bone Regeneration Mediated by Biomimetic Mineralization of a Nanofiber Matrix. *Biomaterials* **2010**, *31*, 6004–6012.
67. Satija, N. K.; Gurudutta, G. U.; Sharma, S.; Afrin, F.; Gupta, P.; Verma, Y. K.; Singh, V. K.; Tripathi, R. P. Mesenchymal Stem Cells: Molecular Targets for Tissue Engineering. *Stem Cells Dev.* **2007**, *16*, 7–23.
68. Song, J. H.; Kim, J. H.; Park, S.; Kang, W.; Kim, H. W.; Kim, H. E.; Jang, J. H. Signaling Responses of Osteoblast Cells to Hydroxyapatite: The Activation of ERK and SOX9. *J. Bone. Miner. Metab.* **2008**, *26*, 138–142.
69. Crowley, J.; Chalivendra, V. B. Mechanical Characterization of Ultra-high Molecular Weight Polyethylene−Hydroxyapatite Nanocomposites. *Biomed. Mater. Eng.* **2008**, *18*, 149–160.
70. Kim, J. Y.; Lee, T. J.; Cho, D. W.; Kim, B. S. Solid Free-Form Fabrication-Based PCL/HA Scaffolds Fabricated with a Multi-head Deposition System for Bone Tissue Engineering. *J. Biomater. Sci. Polym. Ed.* **2010**, *21*, 951–962.
71. Kim, K.; Dean, D.; Lu, A.; Mikos, A. G.; Fisher, J. P. Early Osteogenic Signal Expression of Rat Bone Marrow Stromal Cells Is Influenced by both Hydroxyapatite Nanoparticle Content and Initial Cell Seeding Density in Biodegradable Nanocomposite Scaffolds. *Acta Biomater.* **2011**, *7*, 1249–1264.
72. Paramonov, S. E.; Jun, H. W.; Hartgerink, J. D. Self-Assembly of Peptide−Amphiphile Nanofibers: The Roles of Hydrogen Bonding and Amphiphilic Packing. *J. Am. Chem. Soc.* **2006**, *128*, 7291–7298.
73. Jaiswal, N.; Haynesworth, S. E.; Caplan, A. I.; Bruder, S. P. Osteogenic Differentiation of Purified, Culture-Expanded Human Mesenchymal Stem Cells *in Vitro*. *J. Cell. Biochem.* **1997**, *64*, 295–312.
74. Prockop, D. J.; Phinney, D. G.; Bunnell, B. A. *Mesenchymal Stem Cells: Methods and Protocols*. Humana Press: Totowa, NJ, 2008.
75. Schmittgen, T. D.; Livak, K. J. Analyzing Real-Time PCR Data by the Comparative C(T) Method. *Nat. Protoc.* **2008**, *3*, 1101–1108.